

## Role of myristoylation in modulating PCaP1 interaction with calmodulin

Marco Pedretti<sup>a,1</sup>, Filippo Favretto<sup>a,1</sup>, Francesca Troilo<sup>b</sup>, Moira Giovannoni<sup>c</sup>, Carolina Conter<sup>a</sup>, Benedetta Mattei<sup>c</sup>, Paola Dominici<sup>a</sup>, Carlo Travaglini-Allocatelli<sup>d</sup>, Adele Di Matteo<sup>b,\*</sup>, Alessandra Astegno<sup>a</sup>

<sup>a</sup> Department of Biotechnology, University of Verona, Strada Le Grazie 15, 37134, Verona, Italy

<sup>b</sup> CNR Institute of Molecular Biology and Pathology, P.le Aldo Moro 5, 00185, Rome, Italy

<sup>c</sup> Department of Life, Health and Environmental Sciences, University of L'Aquila, 67100, L'Aquila, Italy

<sup>d</sup> Department of Biochemical Sciences, Sapienza University of Rome, P.le Aldo Moro 5, 00185, Rome, Italy

### ARTICLE INFO

Handling editor: Shivendra Sahi

#### Keywords:

Calcium  
Calmodulin  
PCaP1  
Arabidopsis  
Myristoylation  
Protein-protein interaction  
Calcium affinity

### ABSTRACT

Plasma membrane-associated Cation-binding Protein 1 (PCaP1) belongs to the plant-unique DREPP protein family with largely unknown biological functions but ascertained roles in plant development and calcium ( $\text{Ca}^{2+}$ ) signaling. PCaP1 is anchored to the plasma membrane via N-myristoylation and a polybasic cluster, and its N-terminal region can bind  $\text{Ca}^{2+}$ /calmodulin (CaM). However, the molecular determinants of PCaP1- $\text{Ca}^{2+}$ -CaM interaction and the functional impact of myristoylation in the complex formation and  $\text{Ca}^{2+}$  sensitivity of CaM remained to be elucidated. Herein, we investigated the direct interaction between Arabidopsis PCaP1 (AtPCaP1) and CaM1 (AtCaM1) using both myristoylated and non-myristoylated peptides corresponding to the N-terminal region of AtPCaP1. ITC analysis showed that AtCaM1 forms a high affinity 1:1 complex with AtPCaP1 peptides and the interaction is strictly  $\text{Ca}^{2+}$ -dependent. Spectroscopic and kinetic  $\text{Ca}^{2+}$  binding studies showed that the myristoylated peptide dramatically increased the  $\text{Ca}^{2+}$ -binding affinity of AtCaM1 and slowed the  $\text{Ca}^{2+}$  dissociation rates from both the C- and N-lobes, thus suggesting that the myristoylation modulates the mechanism of AtPCaP1 recognition by AtCaM1. Furthermore, NMR and CD spectroscopy revealed that the structure of both the N- and C-lobes of  $\text{Ca}^{2+}$ -AtCaM1 changes markedly in the presence of the myristoylated AtPCaP1 peptide, which assumes a helical structure in the final complex. Overall, our results indicate that AtPCaP1 biological function is strictly related to the presence of multiple ligands, i.e., the myristoyl moiety,  $\text{Ca}^{2+}$  ions and AtCaM1 and only a full characterization of their equilibria will allow for a complete molecular understanding of the putative role of PCaP1 as signal protein.

### 1. Introduction

Calcium ( $\text{Ca}^{2+}$ ) is a crucial intracellular messenger in all eukaryotic organisms; in plants,  $\text{Ca}^{2+}$  signaling is involved in many events, such as cellular and developmental processes, response to biotic and abiotic stress, symbioses with rhizobial bacteria and mycorrhizal fungi, and immunity (Yang et al., 2003; Kudla et al., 2010, 2018; DeFalco et al., 2010; Oldroyd et al., 2008; Köster et al., 2022). The free cytosolic  $\text{Ca}^{2+}$ , which is kept at a low concentration (~50–200 nM) in the resting state, rapidly increases upon stimuli perception due to the entry of  $\text{Ca}^{2+}$  from external and internal stores in a spatially and temporally controlled manner (Pirayesh et al., 2021; Lee et al., 2021). Afterward,  $\text{Ca}^{2+}$ -binding sensor proteins transduce the  $\text{Ca}^{2+}$  signals into the downstream

responses by reversibly binding  $\text{Ca}^{2+}$  and interacting with various targets (Pirayesh et al., 2021; Xu et al., 2022). Different  $\text{Ca}^{2+}$  sensors exist in plants, such as calmodulins (CaM) and calmodulin-like-proteins (CMLs) (Astegno et al., 2016, 2017; Ogunrinde et al., 2017; La Verde et al., 2018a, 2018b; Dobney et al., 2009; Trande et al., 2019; Leba et al., 2012; Cho, 2016; Vallone et al., 2016; Vandelle et al., 2018),  $\text{Ca}^{2+}$ -dependent protein kinases (CDPKs) and calcineurin B-like proteins (CBLs) (DeFalco et al., 2010; Kudla et al., 2018; Edel et al., 2015), suggesting a high level of sub-functionalization and specificity in plants with respect to the animal counterpart.

CaM is one of the most conserved regulatory proteins in all eukaryotes. Seven CaM genes, encoding for four isoforms that share 90–100% primary sequence identity, were identified in the *Arabidopsis thaliana*

\* Corresponding author.

E-mail address: [adele.dimatteo@cnr.it](mailto:adele.dimatteo@cnr.it) (A. Di Matteo).

<sup>1</sup> These authors contributed equally.

<https://doi.org/10.1016/j.plaphy.2023.108003>

Received 16 March 2023; Received in revised form 9 August 2023; Accepted 4 September 2023

Available online 9 September 2023

0981-9428/© 2023 The Authors.

Published by Elsevier Masson SAS. This is an open access article under the CC BY license (<http://creativecommons.org/licenses/by/4.0/>).

genome (McCormack et al., 2003, 2005). CaM has a dumbbell-like structure consisting of two domains (the N- and C-lobes) connected by a flexible helix (McCormack et al., 2003; Perochon et al., 2011). Each globular domain contains two EF-hands that reversibly bind  $\text{Ca}^{2+}$  in a cooperative manner (La Verde et al., 2018b; Gifford et al., 2007). Binding of  $\text{Ca}^{2+}$  ions to CaM induces significant conformational changes resulting in the exposure of large hydrophobic grooves that usually mediate the target recognition (Astegno et al., 2016; Tidow et al., 2013; Gifford et al., 2013).

The Cation binding Protein 1 (PCaP1), also known as Microtubule-Destabilizing Protein 25 (MDP25), belongs to plant-specific Developmentally Regulated Plasma membrane Polypeptide (DREPP) family whose members interact with the plasma membrane (PM) and are differentially regulated during plant development (Vosolsobè et al., 2017). PCaP1 regulates many processes in plant life, such as microtubule organization, stomatal closure, root hydrotropism, and viral cell-to-cell movement (Yang et al., 2022; Nagata et al., 2016; Li et al., 2011; Qin et al., 2012; Vijayapalani et al., 2012). Moreover, PCaP1 was demonstrated to be involved in elicitor-induced plant immune response by either specific endogenous Damage-Associated Molecular Patterns (DAMPs), i.e., oligogalacturonides (OGs), and Pathogen-Associated Molecular Patterns, i.e., flagellin (flg22) (Giovannoni et al., 2021). These findings are in line with previous studies on elicitor-induced phosphoproteome changes of *Arabidopsis thaliana* that revealed PCaP1 as phosphoregulated in response to both OGs and flg22 (Mattei et al., 2016; Rayapuram et al., 2014).

PCaP1 from *A. thaliana* (AtPCaP1) is a hydrophilic,  $\text{Ca}^{2+}$ -binding protein (Ide et al., 2007) composed of 225 residues with no obvious functional domain. It is anchored to the PM through both N-myristoylation at Gly2 and a relatively strong polybasic amino acid cluster in the N-terminal region that contribute to the interaction with phosphatidylinositol phosphates (PtdInsPs) (Vosolsobè et al., 2017; Kato et al., 2010; Nagasaki et al., 2008). Recently, AtPCaP1 was found to bind uranyl which induces protein oligomerization (Vallet et al., 2023). Furthermore, AtPCaP1 interacts with CaM, and the presence of  $\text{Ca}^{2+}$ -CaM impairs the interaction of AtPCaP1 with PtdInsPs in a competitive manner (Kato et al., 2010; Nagasaki et al., 2008). The involvement of the N-terminal region in recognition of CaM and interaction with PtdInsPs was recently demonstrated also for the *Arabidopsis* isoform PCaP2, which is highly homologous to AtPCaP1 (25% overall primary sequence identity; 70% identity of the N-terminal region) (Kato et al., 2013), thus supporting a functional role of the AtPCaPs-CaM interaction in the transduction of the  $\text{Ca}^{2+}$  signals (Giovannoni et al., 2021; Ide et al., 2007; Kato et al., 2010, 2013; Tanaka-Takada et al., 2019). However, the molecular determinants of AtPCaP-CaM interaction and the role of myristoylation in the complex formation remain to be elucidated.

Here, we identified the specific CaM-binding site within the N-terminus of AtPCaP1 and investigated the *in vitro* properties of the interaction between myristoylated (myr) and non-myristoylated (non-myr) peptides corresponding to this site and the *Arabidopsis* CaM1 (AtCaM1) to clarify which roles AtCaM1 might play in AtPCaP1 regulation. The results obtained suggested that the N-terminal myristoylated region is directly involved in the AtPCaP1-AtCaM1 interaction, providing new insights into the interplay between AtCaM1 and AtPCaP1 in  $\text{Ca}^{2+}$ -mediated signaling processes in plants.

## 2. Materials and methods

### 2.1. Proteins production and peptide synthesis

AtCaM1 and its mutants B12Q-AtCaM1 (E32Q-E68Q) and B34Q-AtCaM1 (E105Q-E141Q) were generated and purified as described in (Astegno et al., 2016; Gut et al., 2009). Uniformly labeled  $^{15}\text{N}$  or  $^{15}\text{N}$ - $^{13}\text{C}$ -AtCaM1 samples for nuclear magnetic resonance (NMR) experiments were prepared using M9 minimal medium supplemented with

$[^{13}\text{C}]$ -glucose and/or  $[^{15}\text{N}]\text{H}_4\text{Cl}$  at a final concentration of  $4\text{ g L}^{-1}$  and  $1\text{ g L}^{-1}$ , respectively.

Synthetic gene (GenScript USA Inc.) corresponding to the complete cDNA of AtPCaP1 (UniProt Q96262) with a tag of six His at the C-terminus was cloned into pET21b expression vector and the recombinant plasmid was transformed into *E. coli* Rosetta (DE3) expression host cells. The culture was grown at  $37^\circ\text{C}$  to  $\text{OD}_{600}$  of 0.6 and induced with  $0.5\text{ mM}$  IPTG (isopropyl- $\beta$ -D-thiogalactoside) at  $24^\circ\text{C}$  for 16 h. The cells were harvested by centrifugation and resuspended in  $20\text{ mM}$  Tris-HCl pH 7.5,  $500\text{ mM}$  KCl,  $20\text{ mM}$  imidazole,  $10\%$  glycerol,  $1\text{ mM}$  DTT in the presence of protease inhibitor EDTA free. After sonication and centrifugation, the supernatant was applied to a Ni-chelating column equilibrated with  $20\text{ mM}$  Tris-HCl pH 7.5,  $500\text{ mM}$  KCl,  $20\text{ mM}$  imidazole,  $10\%$  glycerol,  $1\text{ mM}$  DTT. Protein elution was performed using a linear gradient from  $20$  to  $500\text{ mM}$  imidazole. Purified protein fractions were pooled and extensively dialyzed in  $50\text{ mM}$  Tris-HCl pH 7.5,  $150\text{ mM}$  KCl,  $0.5\text{ mM}$  DTT buffer to remove imidazole. The homogeneity and purity of the protein were verified by SDS-PAGE.

The myristoylated and non-myristoylated AtPCaP1 peptides (res: 2-GYWNskvvpkfkklFEKNSAKKAAA-26) were synthesized by GenScript USA Inc. The concentration of each peptide was determined using their predicted molar extinction coefficient at  $280\text{ nm}$ .

### 2.2. Isothermal titration calorimetry

Isothermal titration calorimetry (ITC) experiments were performed on a MicroCal PEAQ-ITC instrument (Malvern Ltd., Malvern, UK) at  $25^\circ\text{C}$  following protocols described in (Pedretti et al., 2020). AtCaM1, full-length AtPCaP1 and the AtPCaP1 peptides (non-myr-AtPCaP1p and myr-AtPCaP1p) were solubilized in the same buffer containing  $50\text{ mM}$  KCl,  $50\text{ mM}$  Tris (pH 7.5) in the presence of  $5\text{ mM}$   $\text{CaCl}_2$  or  $5\text{ mM}$  EGTA, filtered and degassed. The pH of the solutions was carefully checked to exclude any pH-variation during ITC experiments. For AtCaM1 - AtPCaP1 peptides interaction,  $200\text{ }\mu\text{L}$  of  $25\text{ }\mu\text{M}$  AtCaM1 was titrated with injections of  $1.5\text{ }\mu\text{L}$  of each peptide ( $300\text{--}400\text{ }\mu\text{M}$ ), with a time gap of  $120\text{ s}$  between each injection. For AtCaM1 - full-length AtPCaP1 interaction,  $200\text{ }\mu\text{L}$  of  $18\text{ }\mu\text{M}$  full-length AtPCaP1 was titrated with injections of  $1.5\text{ }\mu\text{L}$  of AtCaM1 ( $160\text{ }\mu\text{M}$ ), with a time gap of  $120\text{ s}$  between each injection. Following the manufacturer's instructions, a first injection of  $0.4\text{ }\mu\text{L}$  was made, and the first data point was removed in the fitting procedure. Data analysis was performed using the MicroCal ITC Origin 7 Analysis Software (MicroCal, Malvern Ltd., Malvern, UK) to obtain the apparent dissociation constant ( $K_d$ ), the enthalpy changes ( $\Delta H$ ), and the apparent entropy change ( $\Delta S$ ) of the interaction. Results represent mean values  $\pm$  SEM of more than three independent experiments using at least two protein preparations.

### 2.3. Nuclear magnetic resonance spectroscopy

Nuclear Magnetic Resonance (NMR) experiments were performed on a  $600\text{ MHz}$  Bruker Avance III spectrometer equipped with a triple resonance Prodigy cryo-probe (Bruker, Karlsruhe, Germany). All the experiments were performed at  $298\text{ K}$  in  $50\text{ mM}$  Tris,  $50\text{ mM}$  KCl,  $0.5\text{ mM}$  DTT (pH 7.5), supplemented with  $5\%$   $\text{D}_2\text{O}$ . Titration experiments were performed by supplementing the  $\text{Ca}^{2+}$ -bound  $^{15}\text{N}$ -AtCaM1 ( $0.55\text{ mM}$ ) sample with increasing amounts of AtPCaP1p or myr-AtPCaP1p till reaching a final molar ratio of 1:2 ( $^{15}\text{N}$ -AtCaM1:peptide) as described in (Bombardi et al., 2022; Conter et al., 2021).  $^1\text{H}$ - $^{15}\text{N}$ -HSQC (Heteronuclear Single Quantum Correlation spectroscopy) experiments were acquired after each peptide addition with 2048 complex points in the direct dimension and 256 complex points in the indirect dimension. In total, 8 transients were acquired with a recycle delay of  $0.2\text{ s}$ .

The combined  $^1\text{H}$ - $^{15}\text{N}$  Chemical shift perturbation (CSP) was calculated in agreement with the following equation:

$$CSP = \sqrt{\frac{(\Delta H)^2 + \left(\frac{\Delta N}{5}\right)^2}{2}} \quad (1)$$

Sequence-specific backbone resonance assignment of  $^{15}\text{N}$ - $^{13}\text{C}$ -AtCaM1 in its  $\text{Ca}^{2+}$ -bound form in the presence or absence of AtPCaP1 peptides was achieved by recording sequential 3D HNCA, HNCACO, HNCACB, HNCO experiments, selected from the Bruker library, using 20% of randomly spread data points (Sattler et al., 1999; Schmieder et al., 1994). The sequential assignment was confirmed with a 3D  $^{15}\text{N}$ -edited NOESY-HSQC experiment selected from the Bruker library, acquired with a matrix of 2048(F3) x 64(F2) x 128(F1) complex points and 16 transients, with a recycle delay of 1.2 s.

Backbone assignment was performed by recording a standard 3D  $^1\text{H}$ - $^{15}\text{N}$  NOESY-HSQC selected from the Bruker library. The experiment was acquired with a matrix of 2048(F3) x 64(F2) x 128(F1) complex points and 16 transients, with a recycle delay of 1.2 s.

All the spectra were processed using the software Topspin (Bruker) and NMRpipe (Delaglio et al., 1995) and successively analyzed with the program ccpnmr Analysis 2.2.1 (Vranken et al., 2005). Non uniform sampling (NUS) experiments were processed using the Sparse multidimensional iterative lineshape-enhanced (SMILE) reconstruction algorithm integrated in NMRpipe (Ying et al., 2017). Backbone assignment of  $\text{Ca}^{2+}$  bound AtCaM1 has been deposited into the BioMagResBank (BMRB) (BMRB entry 52071).

#### 2.4. Circular dichroism spectroscopy

Far-UV circular dichroism (CD) spectra at 25 °C were recorded between 200 (or 190) and 250 nm using 0.1 cm quartz cuvettes on a Jasco J-1500 spectropolarimeter equipped with a temperature control device. Protein and peptide samples were dissolved in a buffer containing 50 mM Tris-HCl, 150 mM KCl, 0.5 mM DTT (pH 7.5) and supplemented with 5 mM  $\text{CaCl}_2$ . Spectra were collected as an average of three scans as previously described (Bombardi et al., 2022; Spyraakis et al., 2011).

#### 2.5. $\text{Ca}^{2+}$ binding assay with chromophoric chelator

The binding of  $\text{Ca}^{2+}$  to AtCaM1 in the absence or presence of AtPCaP1 peptides was studied by 5,5'-Br<sub>2</sub>-BAPTA [5,5'-dibromobis-(o-aminophenoxy) ethane N,N,N',N'-tetra-acetic acid] competition essay (Andre et al., 2002; Astegno et al., 2014; Linse et al., 1991). Briefly, the decrease in the absorbance ( $\lambda = 263$  nm) of 25  $\mu\text{M}$  5,5'-Br<sub>2</sub>-BAPTA ( $\text{Ca}^{2+}$  affinity = 2.3  $\mu\text{M}$  in 0.15 M KCl) in the presence of 25  $\mu\text{M}$  AtCaM1 was followed upon addition of 3  $\mu\text{M}$   $\text{Ca}^{2+}$  for each titration point at 25 °C. Decalcified proteins were solubilized in decalcified 50 mM Tris-HCl pH 7.5, 150 mM KCl buffer (initial  $\text{Ca}^{2+}$  concentration in the buffer ranged between 0.3 and 0.5  $\mu\text{M}$ ). The stoichiometric ratio AtCaM1: AtPCaP1 peptide was set to 1 : 1.5. Data were normalized as follows:

$$\text{normalized } A = \frac{A_{263} - A_{\min}}{A_{\max} - A_{\min}} \quad (2)$$

where  $A_{263}$  is the absorbance at each titration point,  $A_{\min}$  and  $A_{\max}$  are the absorbance values at the lowest and highest  $\text{Ca}^{2+}$  concentration, respectively.

The normalized signal decrease upon  $\text{Ca}^{2+}$  titration was fitted to a four-site binding model for AtCaM1 (Astegno et al., 2016) using CaLigand (Andre et al., 2002) to estimate individual macroscopic binding constants.

#### 2.6. Kinetic rate measurements

$\text{Ca}^{2+}$  dissociation rate constants from AtCaM1 complexed with AtPCaP1 peptides were measured using the SX-18 stopped-flow apparatus (Applied Photophysics, Leatherhead, UK) taking advantage of the  $\text{Ca}^{2+}$  chelator Quin-2 whose fluorescence changes upon binding of  $\text{Ca}^{2+}$ .

Stopped flow experiments were performed at 11 °C in 50 mM Tris-HCl, 150 mM KCl (pH 7.5) as previously described (Troilo et al., 2022). The change of Quin-2 fluorescence signal as a function of time was monitored using an excitation wavelength  $\lambda_{\text{ex}} = 332$  nm, and a 435 nm emission cut-off filter. Solutions of 6  $\mu\text{M}$  AtCaM1 or AtCaM1 variants (B12Q and B34Q) and 18  $\mu\text{M}$  AtPCaP1 or myr-AtPCaP1 peptides, in 50  $\mu\text{M}$   $\text{Ca}^{2+}$ , were rapidly mixed with 150  $\mu\text{M}$  Quin-2.

For each trace, data from 4 to 8 injections were averaged and fitted with either a single (Eq (3)) or double (Eq (4)) exponential function.

$$F = a \times e^{(-k_{\text{obs}} \times t)} + F_{\text{max}} \quad (3)$$

Where  $F$  is the observed fluorescence intensity at time  $t$ ;  $a$  is the amplitude of the fluorescence change;  $k_{\text{obs}}$  is the rate constant at which the change in fluorescence is occurring, representing the  $\text{Ca}^{2+}$  dissociation rate ( $k_{\text{off}}$ ) from the proteins; and  $F_{\text{max}}$  is the fluorescence signal at infinite time.

$$F = a_1 \times e^{(-k_{\text{obs}1} \times t)} + a_2 \times e^{(-k_{\text{obs}2} \times t)} + F_{\text{max}} \quad (4)$$

Where:  $a_1$  and  $a_2$  are the individual amplitudes of each component of the fluorescence change;  $k_{\text{obs}1}$  and  $k_{\text{obs}2}$  are the corresponding rate constants.

Data were normalized to maximum (1) and minimum (0) fluorescence. Graphs were obtained using Prism-GraphPad 6. All the traces were fitted excluding data points in the dead-time of the stopped-flow (<2 ms).

### 3. Results

#### 3.1. Identification of CaM-binding site in AtPCaP1

A putative CaM-binding region was identified in the first 26 N-terminal amino acids ( $^2\text{GYWNSKVVVPFKKLFKNSAKKAAA}^{26}$ ) of the AtPCaP1 sequence using the Calmodulin Target Database (Yap et al., 2000). This region possesses the typical 1–8–14 motif, and an  $\alpha$ -helical wheel representation of the predicted sequence shows that the positively charged residues are located on one side of the wheel, while the hydrophobic amino acids are on the other side when the peptide forms an  $\alpha$ -helical structure (Fig. 1A) (Tidow et al., 2013). Peptides mimicking this putative CaM-binding domain in AtPCaP1 (AtPCaP1p) were synthesized in both myristoylated (at Gly2) and non-myristoylated forms. The far-UV CD spectra of AtPCaP1p (Fig. 1B) and myr-AtPCaP1p (Fig. S1A) recorded in the presence of varying amounts of 2,2,2-Trifluoroethanol (TFE) confirmed that they have a strong propensity to form  $\alpha$ -helical structures. TFE strengthens the hydrogen bonding inducing and stabilizing  $\alpha$ -helices in sequences with helical propensity, therefore mimicking the hydrophobic environment of these regions in the intact protein. In aqueous solution, the AtPCaP1 peptides were largely unstructured with a CD spectrum characterized by a negative peak centered around 200 nm (Fig. 1B and Fig. S1A). However, when the TFE concentration was increased to 20% v/v, the peptides adopted an  $\alpha$ -helical structure, with two peaks at 208 and 222 nm. The helical content further increased at higher [TFE], thus confirming the ability of peptides to acquire  $\alpha$ -helical conformation in hydrophobic environments.

Since in most CaM-peptide interactions, the peptide undergoes a major secondary structure rearrangement from a random coil, flexible structure when isolated to an  $\alpha$ -helix structure upon complex formation, we next explored this aspect in the AtCaM1-AtPCaP1p interaction using CD spectroscopy. The far-UV CD spectrum of AtCaM1 is typical of an  $\alpha$ -helical protein (Astegno et al., 2014, 2016), while the free peptides appear to be unstructured (Fig. 1C and Fig. S1B). However, the addition of AtPCaP1 peptides is accompanied by an increase in the dichroic signal, which can be attributed to a coil-to-helix transition of the peptide as it binds to AtCaM1 (Fig. 1C and Fig. S1B), as reported for many other CaM-target peptides (Astegno et al., 2016, 2017; La Verde et al., 2018a). Overall, these analyses clearly indicate that the first 26

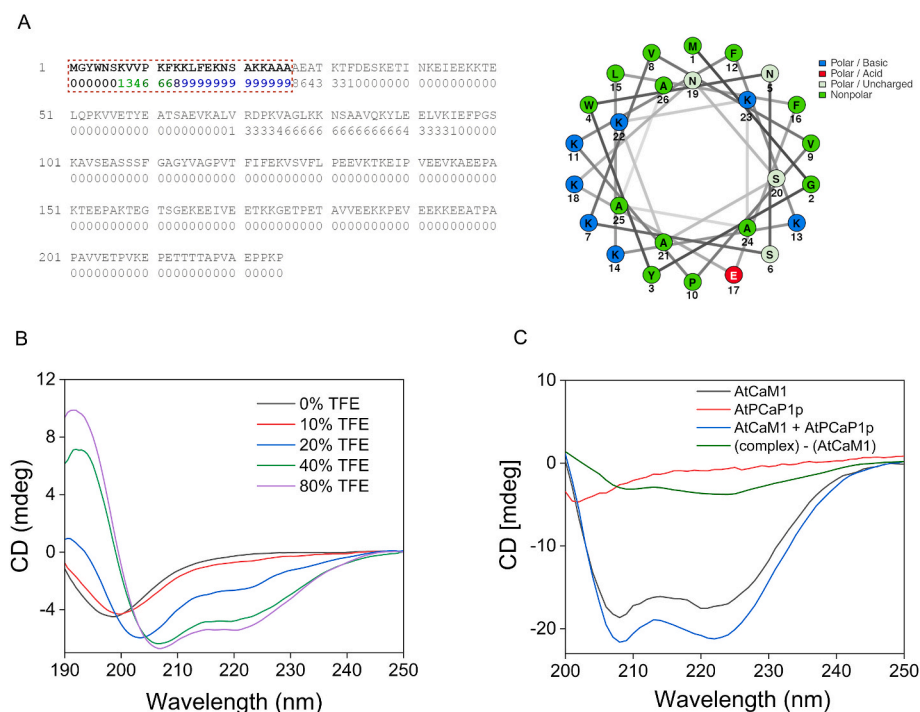


**Fig. 1.** Analysis of CaM binding region of AtPCaP1. (A) The primary sequence of AtPCaP1 is reported together with the CaM binding score obtained by the Calmodulin Target Database search (Yap et al., 2000) and the wheel model of the first 26 N-terminal residues. (B) CD spectra of AtPCaP1p (in aqueous solution or at different [TFE] mixtures). (C) CD spectra of AtCaM1 (black line) and AtPCaP1p (red line), and the protein-peptide complex (blue line) in the presence of 5 mM  $\text{CaCl}_2$ . The green line results from subtracting the blue line (complex) and the black line (AtCaM1). All spectra were recorded using  $0.2 \text{ mg mL}^{-1}$  of AtCaM1. For the complex, a 1:2 M ratio of the peptide was added.

residues of AtPCaP1 possess the features of the typical CaM-binding motifs.

### 3.2. Thermodynamics of AtCaM1-AtPCaP1 interaction

The energetics of AtPCaP1 peptides binding to AtCaM1 were studied using isothermal titration calorimetry (ITC). The thermodynamic parameters of the interaction are reported in Table 1. Representative thermograms and the binding curves for the titration of AtPCaP1p or myr-AtPCaP1p into AtCaM1 in the presence of  $\text{Ca}^{2+}$  or EGTA are shown in Fig. 2.

Our data showed that in the presence of  $\text{Ca}^{2+}$ , all the binding reactions take place with an exothermic heat exchange (negative enthalpy) and a 1:1 stoichiometry. For the  $\text{Ca}^{2+}$ -AtCaM1-AtPCaP1p couple, the experimental data could be best fitted to a one-site binding model, giving a dissociation constant ( $K_d$ ) of  $911 \pm 63 \text{ nM}$ . Notably, the presence of the myristoyl-group at Gly2 significantly enhances the affinity of AtCaM1 for the peptide ( $K_d = 66 \pm 12 \text{ nM}$ ). In contrast, no significant binding of AtPCaP1 peptides to AtCaM1 was detected in the absence of  $\text{Ca}^{2+}$  (i.e., in the presence of the metal chelator EGTA), thus indicating the strong dependence on  $\text{Ca}^{2+}$  of the AtCaM1-AtPCaP1 interaction. The negative  $T\Delta S$  value (Table 1), which is largely compensated by the negative enthalpic contribution of the reaction, confirmed a conformational rearrangement of AtPCaP1 peptides to an ordered helix upon binding to AtCaM1 as shown by CD spectroscopic analysis (Fig. 1).

**Table 1**  
Thermodynamic parameters of the interaction between AtCaM1 and AtPCaP1 peptides in the presence of 5 mM  $\text{CaCl}_2$  at  $25^\circ\text{C}$ . The reported parameters are the mean  $\pm$  standard error of the mean (SEM) of at least three independent titrations using two different protein preparations.

	n	$K_d$ (nM)	$\Delta H$ (kcal mol $^{-1}$ )	$-T\Delta S$ (kcal mol $^{-1}$ )
$\text{Ca}^{2+}$ /AtCaM1 + myr-AtPCaP1p	$0.9 \pm 0.1$	$66 \pm 12$	$-12.5 \pm 0.8$	$2.7 \pm 0.8$
$\text{Ca}^{2+}$ /AtCaM1 + AtPCaP1p	$1.1 \pm 0.0$	$911 \pm 63$	$-17.0 \pm 0.5$	$8.7 \pm 0.5$

We also produced the recombinant full-length AtPCaP1 in *E. coli* and purified it to homogeneity, as evidenced by SDS-PAGE (Fig. S2A). The structural integrity of the protein was further validated through far-UV CD analysis, which revealed a characteristic spectrum indicative of a protein with alpha helix content, displaying double minima at 208 and 222 nm (Fig. S2B).

The thermodynamic properties of the interaction between the full-length AtPCaP1 (in the non-myristoylated form) and AtCaM1 was studied by ITC in the presence of  $\text{Ca}^{2+}$  or EGTA. ITC data (Fig. S3 and Table S1) showed that the AtPCaP1-AtCaM1 interaction is a  $\text{Ca}^{2+}$ -dependent exothermic binding reaction with a favorable enthalpy ( $-9.4 \pm 0.5 \text{ kcal mol}^{-1}$ ) but an unfavorable entropy ( $1.1 \pm 0.4 \text{ kcal mol}^{-1}$ ). The dissociation constant ( $K_d$ ) for the complex is  $859 \pm 62 \text{ nM}$  and the stoichiometry is  $0.8 \pm 0.1$ , indicating high affinity 1:1 complex formation (Table S1). In the presence of EGTA, no binding was observed.

ITC results obtained with the full-length AtPCaP1 are consistent with those obtained using the non-myristoylated peptide approach; this provides strong evidence that the N-terminal region of AtPCaP1 fully recapitulates the interaction of AtPCaP1 with AtCaM1, making it a suitable representative model for further studies.

### 3.3. The myristoyl moiety has a significant effect on the conformation of the AtCaM1-AtPCaP1 complex

An NMR-based approach was used to structurally characterize  $\text{Ca}^{2+}$ -AtCaM1 when bound to AtPCaP1 peptides. We collected two-dimensional  $^1\text{H}$ ,  $^{15}\text{N}$ -HSQC NMR spectra of  $^{15}\text{N}$ -labeled  $\text{Ca}^{2+}$ -AtCaM1 in the absence and presence of unlabeled AtPCaP1 peptides. As shown in Fig. 3A, several resonances of AtCaM1 underwent significant chemical shift perturbation (CSP) and intensity variation following the addition of both myr and non-myristoylated peptides, indicating the physical interaction between the protein and the peptides and the formation of a well-organized  $\text{Ca}^{2+}$ -protein-peptide complex.

To further investigate the structural basis of AtCaM1 interaction with AtPCaP1 peptides, we assigned the backbone chemical shifts of free  $\text{Ca}^{2+}$ -AtCaM1 and  $\text{Ca}^{2+}$ -AtCaM1 when bound to myristoylated and non-myristoylated AtPCaP1 peptides (Fig. S4). The chemical shift assignments were obtained using standard double- and triple-resonance NMR experiments

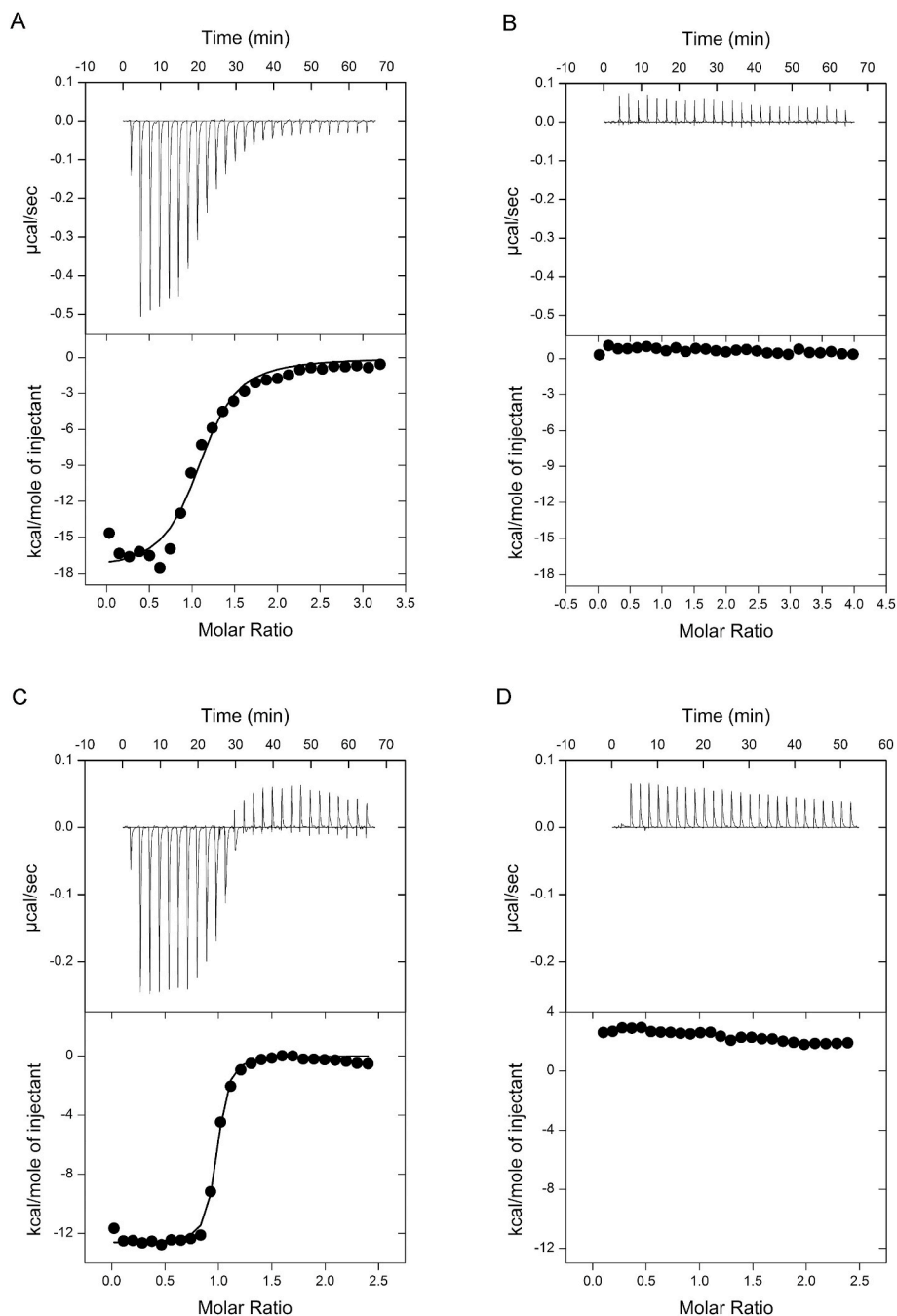


**Fig. 2.** AtPCaP1 peptides binding to AtCaM1 studied by ITC in the presence and absence of  $\text{Ca}^{2+}$ . Representative thermograms (top panels) and the derived binding isotherms (bottom panels) of titration of AtPCaP1p (A, B) and myr-AtPCaP1p (C, D) into AtCaM1 in the presence of 5 mM  $\text{CaCl}_2$  (A, C) or 5 mM EGTA (B, D) at 25 °C. The ligand dilution blank experiment (peptide titrated into buffer) was subtracted from the binding isotherm obtained in the presence of protein. A first injection of 0.4  $\mu\text{L}$  was made, and the first data point was removed from the data fitting.

conducted on uniformly  $^{15}\text{N}$ - and  $^{13}\text{C}/^{15}\text{N}$ -labeled protein samples. The goodness of the assignment was also confirmed using a 3D  $^{15}\text{N}$ -edited NOESY, a technique that provides information on nuclei closed in space (usually  $\sim 5\text{--}6$  Å) and by comparing the NMR resonances of  $\text{Ca}^{2+}$ -AtCaM1 from different species that have been previously assigned by several groups (Ikura et al., 1990, 1992; Chou et al., 2001). The backbone chemical shifts of AtCaM1 were assigned with 97% completion for free  $\text{Ca}^{2+}$ -AtCaM1 and  $\text{Ca}^{2+}$ -AtCaM1 in complex with the non-myr AtPCaP1 peptide, excluding the two Pro residues and the first three N-terminal residues (Met, Ala, and Asp), due to their intrinsic flexibility. Instead, upon addition of myr-AtPCaP1p several resonances underwent significant CSP and signal broadening, thus we could assign approximately the 87% of the signals present in the  $^{15}\text{N}$ -HSQC spectrum.

Structural changes in  $\text{Ca}^{2+}$ -AtCaM1 induced upon peptide binding were probed by comparing the backbone  $^1\text{H}$  and  $^{15}\text{N}$  chemical shifts of

free  $\text{Ca}^{2+}$ -AtCaM1 and  $\text{Ca}^{2+}$ -AtCaM1 bound to each peptide. Differences in these chemical shifts were quantified and the CSPs plotted as a function of residue number (Fig. 3B). Notably, the degree and the extent of backbone CSPs were markedly different in our two protein-peptide complexes (Fig. 3B–D). Upon addition of myr-AtPCaP1p to AtCaM1, most of the  $^{15}\text{N}$ -AtCaM1 resonances that underwent extensive chemical shift changes ( $>0.2$  ppm) were dispersed throughout the protein backbone and were present within both the N- and C-terminus of the  $^{15}\text{N}$ -AtCaM1 sample, suggesting that a global conformational transition of AtCaM1 occurs upon binding of the myr-peptide (Fig. 3B and C). In particular, the region spanning from residue I64–K74 corresponding to the linker between the N-terminal and C-terminal lobes shifted significantly with an average CSP of  $\sim 0.35$  ppm. We also noticed that many hydrophobic residues namely F20, V56, F93, V109, M110, N111, L112 and M146 disappeared from the spectrum after peptide binding and

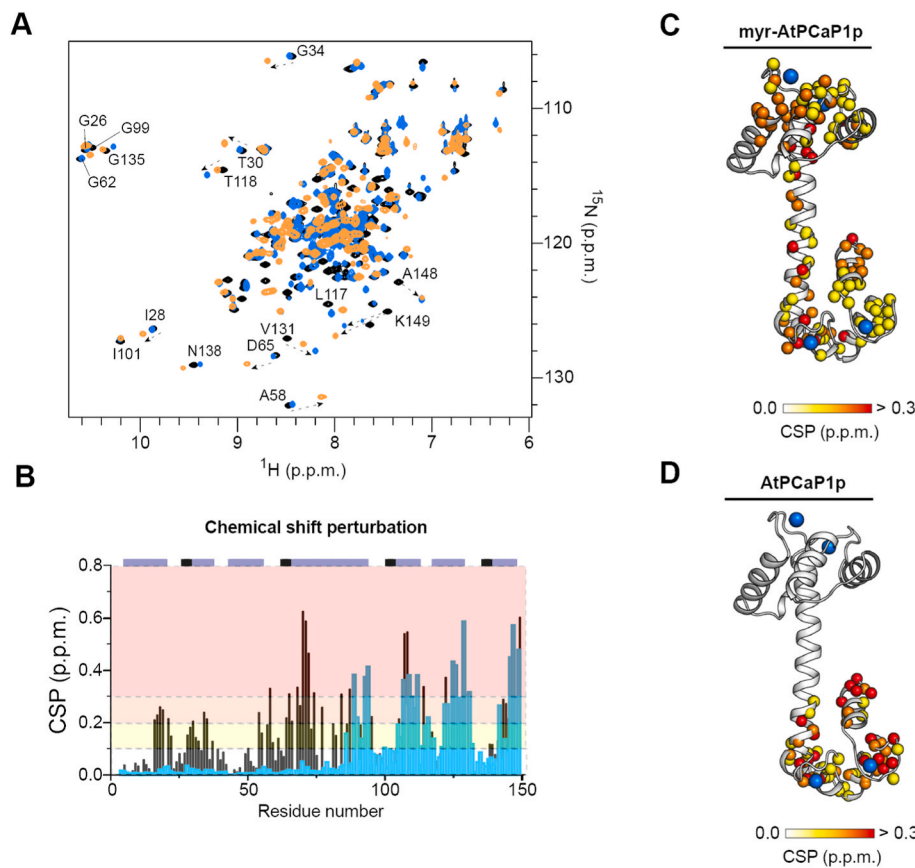


**Fig. 3. Interaction between AtCaM1 and AtPCaP1 peptides revealed by NMR.** (A) Overlaid HSQC spectra of  $\text{Ca}^{2+}$ -AtCaM1 (black) with  $\text{Ca}^{2+}$ -AtCaM1-AtPCaP1p (light blue) or  $\text{Ca}^{2+}$ -AtCaM1-myr-AtPCaP1p (orange). A subset of assigned peaks displaying significant movement upon peptide binding are indicated. (B) Backbone amide  $^1\text{H}$  and  $^{15}\text{N}$  CSPs induced by the binding of either non-myr (light blue) or myr-AtPCaP1p (black) to  $\text{Ca}^{2+}$  saturated AtCaM1 as a function of amino acid residue number. Secondary structural elements, derived from the structure of human CaM in complex with  $\text{Ca}^{2+}$  (PDB:1CLL) are displayed on the top of the figure as  $\alpha$ -helices (grey rectangle) and  $\beta$ -sheets (black rectangle). Regions undergoing significant chemical shift changes are color coded in panels C and D onto the 3D structure of  $\text{Ca}^{2+}$  AtCaM1 from white (CSP <0.1 ppm) to red (CSP >0.3 ppm). (C, D) Three-dimensional representation of perturbed residues in  $\text{Ca}^{2+}$ -AtCaM1 (model calculated using AlphaFold2) upon binding of the synthetic myr-AtPCaP1p (C) or synthetic non-myr AtPCaP1p (D). Residues displaying  $^1\text{H}$ - $^{15}\text{N}$  chemical shift perturbation are mapped as colored spheres on the protein structure from yellow (CSP >0.1 ppm) to red (CSP >0.3 ppm). Residues with a CSP <0.1 ppm are displayed in white.  $\text{Ca}^{2+}$  atoms are displayed as blue spheres.

could not be assigned. These residues were primarily found in the hydrophobic clefts of the N and C-domain of AtCaM1 and seem to be directly involved in the binding of the myristoyl moiety providing hydrophobic contacts in the human CaM (PDB: 1L7Z) (Matsubara et al., 2004).

On the other hand, although a few backbone resonances in the N-lobe and the central linker of AtCaM1 were affected by the binding of non-myr AtPCaP1p, most changes map to AtCaM1's C-lobe (residues 86–149), suggesting a crucial role for the C-terminal domain in the target recognition (Fig. 3B and D).

Notably, inspection of the downfield resonances corresponding to the glycine residues at position six of the four  $\text{Ca}^{2+}$ -binding EF-loops (G26, G62, G99 and G135) revealed that the peaks belonging to G26 (EF-1) and G62 (EF-2) of AtCaM1 remain unperturbed upon non myr-peptide binding, supporting the conclusion that AtCaM1 N-terminal domain is not critically involved in the binding of non-myr AtPCaP1p. On the contrary, all the four peaks corresponding to G26, G62, G99 and G135 were characterized by a clear chemical shift variation upon AtCaM1-myr AtPCaP1p complex formation.

Overall, our NMR data suggest that the binding of the two AtPCaP1 peptides to AtCaM1 results in complexes of different final conformations with the myristoyl group that has a large impact on AtCaM1 conformation.

Moreover, an accurate analysis of NMR titration data for binding of unlabeled AtPCaP1p or myr-AtPCaP1p to  $\text{Ca}^{2+}$ -AtCaM1 indicates that, upon increasing concentrations of peptides, most of the cross-peaks in the  $^1\text{H}$ - $^{15}\text{N}$  HSQC spectrum of  $^{15}\text{N}$ -AtCaM1 display a strong intensity decrease without additional line broadening. This is a classical behavior of resonances in slow exchange on the NMR time scale, which typically corresponds to an intermolecular dissociation constant on the order of  $10^{-7}$  M or less (Latham et al., 2009; Favretto et al., 2020); furthermore, only a single set of AtCaM1 resonances was observed when bound to

peptides, pointing to a 1:1 stoichiometry, in agreement with the above-described ITC results.

We also analyzed the solution properties of the AtCaM1 alone and in complex with both peptides by size exclusion chromatography (SEC) in the presence of  $\text{Ca}^{2+}$  (Fig. S5A). Specifically, the myr-AtPCaP1p-AtCaM1 complex elutes later compared to AtCaM1 alone. This suggests that the binding of the myristoylated peptide induced a conformational change in AtCaM1 that leads to a smaller hydrodynamic radius, likely due to a more compact entity. On the other hand, the AtPCaP1p-AtCaM1 complex elutes earlier than AtCaM1 alone, suggesting a larger hydrodynamic radius for this complex. These observations are consistent with NMR data and support the notion that myr-AtPCaP1p and AtPCaP1p interact with AtCaM1 in different ways, leading to complexes with distinct final conformations.

SEC analysis performed with the full-length AtPCaP1 again recapitulates results obtained with the AtPCaP1 peptide (Fig. S5B). Indeed, the AtPCaP1-AtCaM1 complex elutes earlier than AtCaM1 alone, highlighting the specific and relatively high-affinity binding between these two proteins in the presence of  $\text{Ca}^{2+}$ .

#### 3.4. Effect of AtPCaP1 peptides on AtCaM1 $\text{Ca}^{2+}$ affinity and $\text{Ca}^{2+}$ dissociation kinetics

The effect of AtPCaP1 peptides on the  $\text{Ca}^{2+}$  binding properties of AtCaM1 was quantitatively evaluated using a competition assay based on the  $\text{Ca}^{2+}$  chelator 5,5'-Br<sub>2</sub>-BAPTA, whose absorption decreases upon ion binding (Andre et al., 2002; Linse et al., 1991). Representative  $\text{Ca}^{2+}$  titration curves of AtCaM1 alone and in the presence of AtPCaP1 peptides are shown in Fig. 4. Since AtCaM1 has been demonstrated to possess four  $\text{Ca}^{2+}$  binding sites (Astegno et al., 2014, 2016), data were fitted with a four-site binding model. Titration of AtCaM1 with 5, 5'-Br<sub>2</sub>-BAPTA allowed to calculate an overall  $K_d$  of  $\sim 16$   $\mu\text{M}$  for  $\text{Ca}^{2+}$

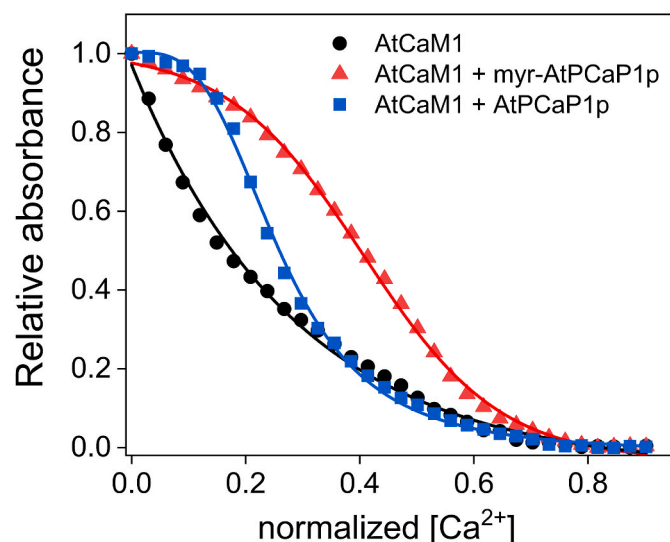


**Fig. 4.**  $\text{Ca}^{2+}$  titration curves obtained by absorption spectroscopy in the presence of the chromophoric  $\text{Ca}^{2+}$  chelator 5,5'-Br<sub>2</sub>-BAPTA. Experimental points for AtCaM1 alone (black circles) and for AtCaM1 in the presence of myr-AtPCaP1p (red triangle) or AtPCaP1p (blue square) are shown together with the optimal curves calculated by computer fitting to a four-states model. Calculated  $\text{Ca}^{2+}$ -binding constants are reported in Table 2; model fitting and data normalization are detailed in the Methods section.

binding to AtCaM1, which is in perfect agreement with the value ( $K_d \sim 13 \mu\text{M}$ ) previously obtained (Table 2) (Astegno et al., 2016). Interestingly, all the four individual macroscopic binding constants significantly changed in the presence of the myr-peptide, revealing an overall  $K_d$  value of  $\sim 180 \text{ nM}$ . Thus, the apparent affinity for  $\text{Ca}^{2+}$  of AtCaM1 was increased of approximately 90-fold in the presence of this peptide. On the other hand, in the presence of the non-myr peptide an apparent  $K_d$  value of  $\sim 0.9 \mu\text{M}$  was measured, such that the affinity for  $\text{Ca}^{2+}$  was increased of only  $\sim 18$ -fold (Table 2). In this case, the most notable changes in macroscopic binding constants were observed only for two out of the four EF-hands ( $K_{d1}$  and  $K_{d2}$ ) (Table 2).

Next, we analyzed the effects of the peptides binding on the kinetics of  $\text{Ca}^{2+}$  dissociation from AtCaM1 by stopped-flow spectroscopy, taking advantage of the fluorescence increase of the  $\text{Ca}^{2+}$  chelator Quin-2 upon  $\text{Ca}^{2+}$  binding. As reported in our previous work, in the absence of targets,  $\text{Ca}^{2+}$  dissociation from the N-lobe of AtCaM1 occurs significantly faster than from the C-lobe ( $k_{\text{obs}} > 500 \text{ s}^{-1}$  and  $k_{\text{obs}} = 15.6 \text{ s}^{-1}$ , respectively, Table 3) (Troilo et al., 2022). Notably, in the presence of both AtPCaP1 peptides, the  $\text{Ca}^{2+}$  dissociation kinetics is a biphasic process (Fig. 5) characterized by two rate constants:  $k_{\text{obs}1} = 3.6 \pm 0.02 \text{ s}^{-1}$  and  $k_{\text{obs}2} = 0.12 \pm 0.005 \text{ s}^{-1}$  with myr-AtPCaP1p (Fig. 5A) and  $k_{\text{obs}1} = 34.6 \pm 0.23 \text{ s}^{-1}$  and  $k_{\text{obs}2} = 0.20 \pm 0.001 \text{ s}^{-1}$  with the non-myr peptide (Fig. 5D, Table 3). To assign the  $\text{Ca}^{2+}$  dissociation rates to each lobe of the protein, we used AtCaM1 mutants deficient in  $\text{Ca}^{2+}$  binding at sites 1 and 2 of the N-lobe (B12Q-AtCaM1) or sites 3 and 4 of the C-lobe (B34Q-AtCaM1) in which only the C-lobe or the N-lobe is competent for  $\text{Ca}^{2+}$  binding, respectively (Troilo et al., 2022).  $\text{Ca}^{2+}$  dissociation from the N-lobe (B34Q-AtCaM1) gives rise to a dissociation rate of  $3.8 \pm 0.01 \text{ s}^{-1}$  and  $28 \pm 0.12 \text{ s}^{-1}$  in the presence of

**Table 2**  
Macroscopic  $\text{Ca}^{2+}$  binding constants for AtCaM1 in the absence and presence of AtPCaP1 peptides.

	$\log K_{a1}$	$K_{d1} (\mu\text{M})$	$\log K_{a2}$	$K_{d2} (\mu\text{M})$	$\log K_{a3}$	$K_{d3} (\mu\text{M})$	$\log K_{a4}$	$K_{d4} (\mu\text{M})$	Overall $K_d$
AtCaM1 <sup>a</sup>	$4.8 \pm 0.1$	15.8	$5.8 \pm 0.2$	1.6	$3.5 \pm 0.2$	316	$5.5 \pm 0.1$	3.2	16 $\mu\text{M}$
AtCaM1 + myr-AtPCaP1p	$8.2 \pm 0.1$	0.006	$6.3 \pm 0.1$	0.5	$6.7 \pm 0.2$	0.2	$5.8 \pm 0.1$	1.6	180 nM
AtCaM1 + AtPCaP1p	$7.1 \pm 0.1$	0.08	$7.4 \pm 0.1$	0.04	$4.2 \pm 0.1$	63	$5.5 \pm 0.2$	3.2	0.9 $\mu\text{M}$

<sup>a</sup> Values from (Astegno et al., 2016).

**Table 3**

$\text{Ca}^{2+}$  dissociation kinetics. The reported parameters are the mean  $\pm$  standard error of the mean (SEM) of at least three independent titrations using two different protein preparations.

	N-lobe	C-lobe
AtCaM1 <sup>a</sup>	$k_{\text{obs}} (\text{s}^{-1})$	$k_{\text{obs}} (\text{s}^{-1})$
B34Q-AtCaM1 <sup>a</sup>	$>500$	$15.6 \pm 0.1$
B12Q-AtCaM1 <sup>a</sup>	$>500$	$14.4 \pm 0.12$
AtCaM1 + myr-AtPCaP1p	$3.6 \pm 0.02$	$0.12 \pm 0.005$
B34Q-AtCaM1 + myr-AtPCaP1p	$3.8 \pm 0.01$	
B12Q-AtCaM1 + myr-AtPCaP1p		$0.24 \pm 0.001$
AtCaM1 + AtPCaP1p	$34.6 \pm 0.23$	$0.2 \pm 0.001$
B34Q-AtCaM1 + AtPCaP1p	$28 \pm 0.12$	
B12Q-AtCaM1 + AtPCaP1p		$0.28 \pm 0.004$

<sup>a</sup> Values from (Troilo et al., 2022).

myr-AtPCaP1p and AtPCaP1p, respectively (Fig. 5B and E, Table 3); while the  $\text{Ca}^{2+}$  dissociation from the C-lobe (B12Q-AtCaM1) results in a  $k_{\text{obs}} = 0.24 \pm 0.001 \text{ s}^{-1}$  in the presence of myr-AtPCaP1p, and  $k_{\text{obs}} = 0.28 \pm 0.004 \text{ s}^{-1}$ , in the presence of AtPCaP1p (Fig. 5C and F, Table 3). Therefore, the binding of both peptides causes an overall decrease in the  $\text{Ca}^{2+}$  dissociation rate constants from both AtCaM1 lobes (N-lobe: from  $>500$  to 3.8 for the myr peptide and to  $28 \text{ s}^{-1}$  for the non-myr peptide, respectively; C-lobe: from 14.4 to 0.24 and  $0.28 \text{ s}^{-1}$  for the myr-AtPCaP1p and AtPCaP1p, respectively) (Table 3) in agreement with the BAPTA experiments which demonstrated an overall increase in the AtCaM1  $\text{Ca}^{2+}$  affinity in the presence of the target peptides. Interestingly, the release of  $\text{Ca}^{2+}$  from the N-lobe occurs  $\cong 7$ -fold faster in the case of AtPCaP1p ( $k_{\text{obs}} = 28 \text{ s}^{-1}$ ) compared to myr-AtPCaP1p ( $k_{\text{obs}} = 3.8 \text{ s}^{-1}$ ) (Table 3).

#### 4. Discussion

PCaP1 belongs to the *Arabidopsis* DREPP family which comprises proteins that interact peripherally with the PM by various mechanisms, including combinations of N-myristoylation and protein-lipid electrostatic interactions due to the presence of a polybasic cluster (Vosolsobé et al., 2017). DREPP proteins have been described as signal proteins and their specific mechanism of PM association has been suggested to be crucial for their localization in signaling platforms in membrane microdomains and thus for their specific function.

According to the AlphaFold model (Fig. S6) more than one-third of the AtPCaP1 protein, particularly the C-terminal region, is predicted to be disordered, while the first 125 residues exhibit  $\alpha$ -helical structure which is consistent with the far-UV CD spectrum of the recombinant protein (Fig. S2B). The structured region of AtPCaP1 is characterized by a central core composed of helices from  $\alpha 3$  to  $\alpha 7$  which is stabilized by hydrophobic interactions. The last part of helix  $\alpha 1$  folds over the central core and, together with  $\alpha 2$ , contributes to capping on one side of the central core. Additionally, the N-terminal portion of the  $\alpha 1$  extends outwards the core. The electrostatic surface of AtPCaP1 shows that helix  $\alpha 1$  has a strong positive charge, and together with three lysine residues located on helix  $\alpha 4$ , it constitutes an extended positively charged surface (Fig. S6).

A closer look at the N-terminal sequence and structural model of AtPCaP1 shows that it contains not only the myristoyl moiety and a polybasic flanking region, which greatly contribute to its interaction

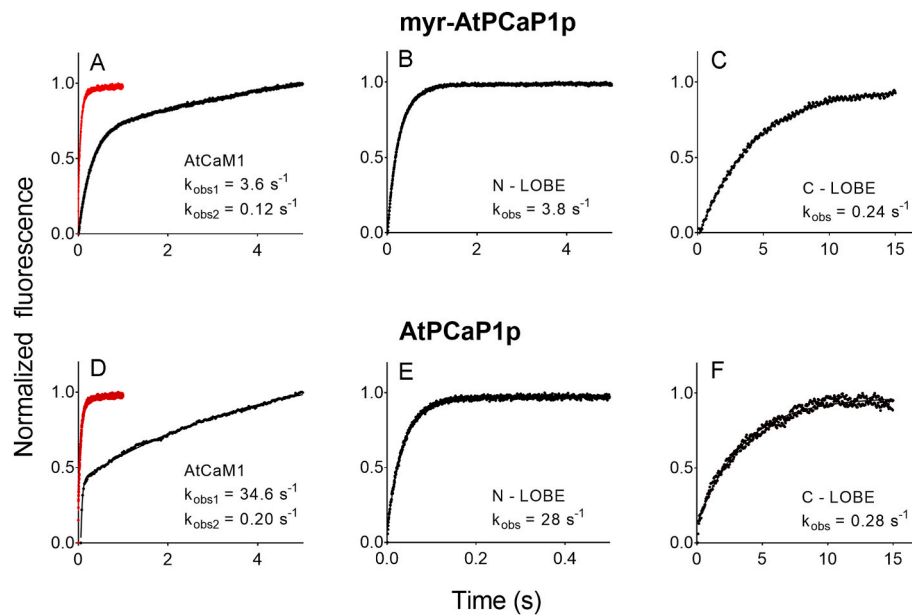


**Fig. 5.** Effect of the AtPCaP1 peptides on Ca<sup>2+</sup> dissociation kinetics from AtCaM1. Time course of Quin-2-induced Ca<sup>2+</sup> dissociation from: AtCaM1 in the absence (red) and presence of myr-AtPCaP1p (A) and AtPCaP1p (D); the N-lobe of AtCaM1 (B34Q variant) in the presence of myr-AtPCaP1p (B) or AtPCaP1p (E); the C-lobe of AtCaM1 (B12Q variant) in the presence of myr-AtPCaP1p (C) or AtPCaP1p (F).

with PM, but it also possesses a 1–8–14 CaM binding motif which is a common recognition motif for Ca<sup>2+</sup>-dependent CaM interactions (Fig. 1A). At physiological Ca<sup>2+</sup> concentrations, the association of PCaP1 with the PM has been shown to be very stable, and not affected by CaM (Nagasaki et al., 2008). Elevated, non-physiological Ca<sup>2+</sup> levels have been shown to cause the partial dissociation of AtPCaP1 from the membrane to the cytosol (Li et al., 2011; Kato et al., 2010; Nagasaki et al., 2008), while for the *M. truncatula* DREPP Ca<sup>2+</sup> treatment caused a relocalization of the protein into nanodomains that colocalize with microtubules (Su et al., 2020), indicating that cytoplasmic Ca<sup>2+</sup> levels are key regulators of the association of DREPP family proteins to the PM. Indeed AtPCaP1, as well as its paralogue AtPCaP2, interacts with Ca<sup>2+</sup>-CaM, and this interaction competitively regulates the binding to PtdInsPs (Li et al., 2011; Kato et al., 2010; Nagasaki et al., 2008), thus adding a further level of sophistication in the fine-tuning of AtPCaP1 associations. However, many questions remain to be answered, such as the definition of the molecular determinants of AtPCaP1-Ca<sup>2+</sup>/CaM interaction, the functional impact of the myristoyl group linked to AtPCaP1 on the complex formation and on the Ca<sup>2+</sup> sensitivity of CaM.

In this work, we investigated the mutual influence of these aspects on the structural and functional properties of the AtPCaP1-AtCaM1 complex formation. We applied an *in vitro* approach that, albeit focused on interactions in which the binding partner AtPCaP1 is reduced to a relatively short peptide, offered valuable insights that enhance and complement other strategies described in the literature (Nagata et al., 2016; Giovannoni et al., 2021; Ide et al., 2007; Vallet et al., 2023; Kato et al., 2013; Tanaka-Takada et al., 2019; Nagasaki-Takeuchi et al., 2008) aimed at unraveling the details of the AtPCaP1- Ca<sup>2+</sup>- AtCaM1 interaction network within plant cells. Notably, although the use of a peptide fragment rather than a whole protein as a AtCaM1 target may result in differences in the Ca<sup>2+</sup>-binding affinity of AtCaM1, our ITC studies failed to detect differences in affinity and stoichiometry when AtCaM1 was in complex with either the peptide corresponding to the CaM-binding domain (the first 26 N-terminal residues) of AtPCaP1 ( $K_d = 911$  nM) or full-length AtPCaP1 ( $K_d = 859$  nM), suggesting that our approach would give representative results and satisfyingly recapitulates the behavior of the entire protein.

We demonstrated that the interaction between AtPCaP1 and AtCaM1 is strictly Ca<sup>2+</sup> dependent and the myristoylation is directly involved in

the association of the two proteins. These findings provide direct support for the proposal of Matsubara and colleagues (Matsubara et al., 2003; Hayashi et al., 2002) that protein myristoylation plays important roles not only in the interaction with membrane phospholipids but also in the protein-protein interaction with Ca<sup>2+</sup>-CaM. In recent years, the interest in the role of myristoylation in plant proteins has increased significantly, although the correlation between the presence of the myristoyl groups and specific functions has been demonstrated only for few proteins, including the Arabidopsis Calcineurin B-like protein 4 (Held et al., 2011), the small G-protein Ara 6 (Yin et al., 2017), and the Pto Kinase protein of Tomato (Andriotis et al., 2006).

Our results, by showing that the myr-AtPCaP1 peptide has an affinity to AtCaM1 about 14-fold higher ( $K_d \sim 60$  nM) than that of the non-myristoylated peptide, suggest that the myristoylation might modulate the mechanism of recognition of AtPCaP1 by AtCaM1 and consequently alter the kinetics of complex formation. Interestingly, several proteins that contain myristoylated polybasic N-terminal sequences, including the brain acid soluble protein 1 (CAP23/NAP22) (Takasaki et al., 1999), the viral proteins negative factor (Nef) from HIV1 (Hayashi et al., 2002), and the oncogenic pp60<sup>v-src</sup> tyrosine-protein kinase from Rous sarcoma virus (Hayashi et al., 2004) have been reported to bind Ca<sup>2+</sup>-CaM.

In the CaM-binding site of these proteins the CaM recognition motif (such as the 1-8-14, 1-5-10, or IQ motif) is absent. As a consequence, binding of these targets to CaM is dependent on the presence of the myristoyl, which, in a linear conformation, occupies the hydrophobic channel formed by the lobes of CaM, while the polybasic amino acid cluster further stabilizes the interaction by contacting the acidic surface of CaM (Grant et al., 2020). In the case of AtPCaP1, the presence of both the myristoyl moiety and a canonical CaM binding motif, in addition to the polybasic cluster (Fig. S6), suggests an additional level of complexity in the mechanism of target recognition by CaM. Our NMR and CD analyses support this conclusion, confirming that the myristoylated AtPCaP1 peptide can bind Ca<sup>2+</sup>-AtCaM1 with 1:1 stoichiometry and high affinity. The overall structure of Ca<sup>2+</sup>-AtCaM1 changes markedly in the presence of the myristoylated AtPCaP1p, and the peptide adopts a helical conformation in the final complex. On the other hand, the binding of AtCaM1 to the non-myristoylated peptide involves mainly local conformational changes at the C-lobe of AtCaM1.

Notably, we observed that the formation of such complexes



significantly increases the AtCaM1 affinity for  $\text{Ca}^{2+}$ . It is well-known that a fine-tuned equilibrium between  $[\text{Ca}^{2+}]$ , CaM, and its target(s) is crucial for the proper biological function, even if it is still unclear how regulation of CaM's affinity for  $\text{Ca}^{2+}$  by target proteins is achieved at the molecular level. Interestingly, a 90-fold and 18-fold increase in affinity for  $\text{Ca}^{2+}$  of AtCaM1 were measured in the presence of the myristoylated and non-myristoylated peptides, respectively, indicating that the myristoylation modulates the  $\text{Ca}^{2+}$  sensitivity of AtCaM1. Significant changes were observed in all the macroscopic binding constants for the four functional EF-hands of AtCaM1 upon the addition of the myristoylated peptide, while in the case of the non-myristoylated one, the most notable changes were observed for the high-affinity sites, which have been previously assigned to the C-lobe of AtCaM1. These results are nicely supported by the NMR data, suggesting that for the myr-AtPCaP1p, the complex formation is mediated by both AtCaM1 lobes, while for the AtPCaP1p, it is mainly mediated by the C-lobe. Measurements of the  $\text{Ca}^{2+}$  dissociation rates from both N- and C-lobes of AtCaM1 showed that  $\text{Ca}^{2+}$  dissociation is remarkably slower in the presence of AtPCaP1 peptides. However, a more significant impact of the myristoyl moiety on the  $\text{Ca}^{2+}$  dissociation from the N-lobe of AtCaM1 was observed, which is likely the cause of the enhanced  $\text{Ca}^{2+}$  affinity ( $\cong$  5-fold) obtained for the complex in the presence of the myristoylated peptide.

AtPCaP1 regulates many important processes in plant life (Nagata et al., 2016; Qin et al., 2012; Tanaka-Takada et al., 2019), viral cell-to-cell movement (Vijayapalani et al., 2012) and immunity (Giovannoni et al., 2021; Mattei et al., 2016). Interestingly, several studies pointed out the role of N-myristoylation in the immune response against microbial and viral infections (Udenwobele et al., 2017; Wang et al., 2021).

It should also be remembered that AtPCaP1 can bind PtdInsPs which are major components of intracellular signaling (Kato et al., 2010). Thus, the interaction between the  $\text{Ca}^{2+}$ -CaM and myristoylated AtPCaP1 represents an important connection between major signaling pathways in plant cells. In this context, our findings allow us to add novel details to the mechanism whereby PCaP proteins act as molecular switches of the  $\text{Ca}^{2+}$  signaling mediated by PPIs and CaM (Kato et al., 2010). It is tempting to speculate that at resting conditions, AtPCaP1 is anchored to the PM via N-myristoylation and a polybasic cluster. When the  $\text{Ca}^{2+}$  concentration increases, the binding to  $\text{Ca}^{2+}$ -CaM stabilizes a suitable helix conformation of the N-terminal region of PCaP1 that would favor myristoyl exposure and subsequent insertion into the hydrophobic clefts of  $\text{Ca}^{2+}$ -CaM. The formation of the final complex decreases the  $\text{Ca}^{2+}$  dissociation rate from AtCaM1, thus ensuring an extended lifetime of the activated protein complex long after the  $[\text{Ca}^{2+}]$  transient has decreased. In parallel, the interaction of AtPCaP1 with  $\text{Ca}^{2+}$ -CaM stimulates the release of PtdInsPs, which may then participate in downstream-specific signaling.

AtPCaP1 is an emerging important player in the cellular  $\text{Ca}^{2+}$  signaling network with multifaceted physiological roles in plant development and immunity. Our data can help to better understand the molecular mechanisms of regulation of these processes by AtPCaP1 and of signal integration by  $\text{Ca}^{2+}$ -AtCaM1.

#### CRedit authorship contribution statement

**Marco Pedretti:** Conceptualization, Formal analysis, Investigation. **Filippo Favretto:** Formal analysis, Investigation. **Francesca Troilo:** Formal analysis, Investigation. **Moira Giovannoni:** Writing – review & editing. **Carolina Conter:** Investigation. **Benedetta Mattei:** Writing – review & editing, Funding acquisition. **Paola Dominici:** Writing – review & editing. **Carlo Travaglini-Allocatelli:** Investigation, Writing – review & editing. **Adele Di Matteo:** Conceptualization, Validation, Writing – original draft, Supervision, Project administration, Funding acquisition. **Alessandra Astegno:** Conceptualization, Validation, Writing – original draft, Supervision, Funding acquisition.

#### Declaration of competing interest

The authors declare that they have no known competing financial interests or personal relationships that could have appeared to influence the work reported in this paper.

#### Data availability

Data will be made available on request.

#### Acknowledgements

This work was supported by the Italian Ministry of University and Research (MIUR) under grant PRIN 2017ZBBYNC funded to AA, AD and BM.

We thank the Centro Piattaforme Tecnologiche of the University of Verona for providing access to the spectroscopic platform.

#### Appendix A. Supplementary data

Supplementary data to this article can be found online at <https://doi.org/10.1016/j.plaphy.2023.108003>.

#### References

- Andre, I., Linse, S., 2002. Measurement of  $\text{Ca}^{2+}$ -binding constants of proteins and presentation of the CaLigand software. *Anal. Biochem.* 305 (2), 195–205.
- Andriotis, V.M., Rathjen, J.P., 2006. The Pto kinase of tomato, which regulates plant immunity, is repressed by its myristoylated N terminus. *J. Biol. Chem.* 281 (36), 26578–26586.
- Astegno, A., et al., 2014. Structural plasticity of calmodulin on the surface of CaF2 nanoparticles preserves its biological function. *Nanoscale* 6 (24), 15037–15047.
- Astegno, A., et al., 2016. Biochemical and biophysical characterization of a plant calmodulin: role of the N- and C-lobes in calcium binding, conformational change, and target interaction. *Biochim. Biophys. Acta, Proteins Proteomics* 1864 (3), 297–307.
- Astegno, A., et al., 2017. Arabidopsis calmodulin-like protein CML36 is a calcium ( $\text{Ca}^{2+}$ ) sensor that interacts with the plasma membrane  $\text{Ca}^{2+}$ -ATPase isoform ACA8 and stimulates its activity. *J. Biol. Chem.* 292 (36), 15049–15061.
- Bombardi, L., et al., 2022. Conformational plasticity of centrin 1 from toxoplasma gondii in binding to the centrosomal protein SFI1. *Biomolecules* 12 (8).
- Cho, K.M., et al., 2016. CML10, a Variant of Calmodulin, Modulates Ascorbic Acid Synthesis. *New Phytol* 209, 664–678.
- Chou, J.J., et al., 2001. Solution structure of  $\text{Ca}^{2+}$ -calmodulin reveals flexible hand-like properties of its domains. *Nat. Struct. Biol.* 8 (11), 990–997.
- Conter, C., et al., 2021. The interplay of self-assembly and target binding in centrin 1 from *Toxoplasma gondii*. *Biochem. J.* 478 (13), 2571–2587.
- DeFalco, T.A., Bender, K.W., Snedden, W.A., 2010. Breaking the code:  $\text{Ca}^{2+}$  sensors in plant signalling. *Biochem. J.* 425 (1), 27–40.
- Delaglio, F., et al., 1995. NMRPipe: a multidimensional spectral processing system based on UNIX pipes. *J. Biomol. NMR* 6 (3), 277–293.
- Dobney, S., et al., 2009. The calmodulin-related calcium sensor CML42 plays a role in trichome branching. *J. Biol. Chem.* 284 (46), 31647–31657.
- Edel, K.H., Kudla, J., 2015. Increasing complexity and versatility: how the calcium signaling toolkit was shaped during plant land colonization. *Cell Calcium* 57 (3), 231–246.
- Favretto, F., et al., 2020. Catalysis of proline isomerization and molecular chaperone activity in a tug-of-war. *Nat. Commun.* 11 (1), 6046.
- Gifford, J.L., Walsh, M.P., Vogel, H.J., 2007. Structures and metal-ion-binding properties of the  $\text{Ca}^{2+}$ -binding helix-loop-helix EF-hand motifs. *Biochem. J.* 405 (2), 199–221.
- Gifford, J.L., et al., 2013. Comparing the calcium binding abilities of two soybean calmodulins: towards understanding the divergent nature of plant calmodulins. *Plant Cell* 25 (11), 4512–4524.
- Giovannoni, M., et al., 2021. The plasma membrane-associated  $\text{Ca}^{2+}$ -binding protein, PCaP1, is required for oligogalacturonide and flagellin-induced priming and immunity. *Plant Cell Environ.* 44 (9), 3078–3093.
- Grant, B.M.M., et al., 2020. Calmodulin disrupts plasma membrane localization of farnesylated KRAS4b by sequestering its lipid moiety. *Sci. Signal.* 13 (625).
- Gut, H., et al., 2009. A common structural basis for pH- and calmodulin-mediated regulation in plant glutamate decarboxylase. *J. Mol. Biol.* 392 (2), 334–351.
- Hayashi, N., et al., 2002. Nef of HIV-1 interacts directly with calcium-bound calmodulin. *Protein Sci.* 11 (3), 529–537.
- Hayashi, N., et al., 2004. Myristoylation-regulated direct interaction between calcium-bound calmodulin and N-terminal region of pp60v-src. *J. Mol. Biol.* 338 (1), 169–180.
- Held, K., et al., 2011. Calcium-dependent modulation and plasma membrane targeting of the AKT2 potassium channel by the CBL4/CIPK6 calcium sensor/protein kinase complex. *Cell Res.* 21 (7), 1116–1130.

- Ide, Y., et al., 2007. Molecular properties of a novel, hydrophilic cation-binding protein associated with the plasma membrane. *J. Exp. Bot.* 58 (5), 1173–1183.
- Ikura, M., Kay, L.E., Bax, A., 1990. A novel approach for sequential assignment of  $^1\text{H}$ ,  $^{13}\text{C}$ , and  $^{15}\text{N}$  spectra of proteins: heteronuclear triple-resonance three-dimensional NMR spectroscopy. Application to calmodulin. *Biochemistry* 29 (19), 4659–4667.
- Ikura, M., et al., 1992. Solution structure of a calmodulin-target peptide complex by multidimensional NMR. *Science* 256 (5057), 632–638.
- Kato, M., et al., 2010. PCaPs, possible regulators of PtdInsP signals on plasma membrane. *Plant Signal. Behav.* 5 (7), 848–850.
- Kato, M., Aoyama, T., Maeshima, M., 2013. The  $\text{Ca}^{2+}$ -binding protein PCaP2 located on the plasma membrane is involved in root hair development as a possible signal transducer. *Plant J.* 74 (4), 690–700.
- Köster, P., DeFalco, T.A., Zipfel, C., 2022.  $\text{Ca}^{2+}$  signals in plant immunity. *EMBO J.* 41 (12), e110741.
- Kudla, J., Batistić, O., Hashimoto, K., 2010. Calcium signals: the lead currency of plant information processing. *Plant Cell* 22 (3), 541–563.
- Kudla, J., et al., 2018. Advances and current challenges in calcium signaling. *New Phytol.* 218 (2), 414–431.
- La Verde, V., et al., 2018a. Binding of calcium and target peptide to calmodulin-like protein CML19, the centrin 2 of *Arabidopsis thaliana*. *Int. J. Biol. Macromol.* 108, 1289–1299.
- La Verde, V., Dominici, P., Astegno, A., 2018b. Towards understanding plant calcium signaling through calmodulin-like proteins: a biochemical and structural perspective. *Int. J. Mol. Sci.* 19 (5).
- Latham, M.P., Zimmermann, G.R., Pardi, A., 2009. NMR chemical exchange as a probe for ligand-binding kinetics in a theophylline-binding RNA aptamer. *J. Am. Chem. Soc.* 131 (14), 5052–5053.
- Leba, L.J., et al., 2012. CML9, a multifunctional *Arabidopsis thaliana* calmodulin-like protein involved in stress responses and plant growth? *Plant Signal. Behav.* 7 (9), 1121–1124.
- Lee, H.-J., Seo, P.-J., 2021.  $\text{Ca}^{2+}$  talyzing initial Responses to environmental stresses. *Trends Plant Sci.* 26 (8), 849–870.
- Li, J., et al., 2011. MDP25, A novel calcium regulatory protein, mediates hypocotyl cell elongation by destabilizing cortical microtubules in *Arabidopsis*. *Plant Cell* 23 (12), 4411–4427.
- Linse, S., Helmersson, A., Forsen, S., 1991. Calcium binding to calmodulin and its globular domains. *J. Biol. Chem.* 266 (13), 8050–8054.
- Matsubara, M., et al., 2003. Direct involvement of protein myristoylation in myristoylated alanine-rich C kinase substrate (MARCKS)-calmodulin interaction. *J. Biol. Chem.* 278 (49), 48898–48902.
- Matsubara, M., et al., 2004. Crystal structure of a myristoylated CAP-23/NAP-22 N-terminal domain complexed with  $\text{Ca}^{2+}$ /calmodulin. *EMBO J.* 23 (4), 712–718.
- Mattel, B., et al., 2016. Comprehensive analysis of the membrane phosphoproteome regulated by oligogalacturonides in *Arabidopsis thaliana*. *Front. Plant Sci.* 7.
- McCormack, E., Braam, J., 2003. Calmodulins and related potential calcium sensors of *Arabidopsis*. *New Phytol.* 159 (3), 585–598.
- McCormack, E., Tsai, Y.C., Braam, J., 2005. Handling calcium signaling: *Arabidopsis* CaMs and CMLs. *Trends Plant Sci.* 10 (8), 383–389.
- Nagasaki, N., Tomioka, R., Maeshima, M., 2008. A hydrophilic cation-binding protein of *Arabidopsis thaliana*, AtPCaP1, is localized to plasma membrane via N-myristoylation and interacts with calmodulin and the phosphatidylinositol phosphates PtdIns(3,4,5)P(3) and PtdIns(3,5)P(2). *FEBS J.* 275 (9), 2267–2282.
- Nagasaki-Takeuchi, N., Miyano, M., Maeshima, M., 2008. A plasma membrane-associated protein of *Arabidopsis thaliana* AtPCaP1 binds copper ions and changes its higher order structure. *J. Biochem.* 144 (4), 487–497.
- Nagata, C., et al., 2016. A novel-type phosphatidylinositol phosphate-interactive, Ca-binding protein PCaP1 in *Arabidopsis thaliana*: stable association with plasma membrane and partial involvement in stomata closure. *J. Plant Res.* 129 (3), 539–550.
- Ogunrinde, A., et al., 2017. *Arabidopsis* calmodulin-like proteins, CML15 and CML16 possess biochemical properties distinct from calmodulin and show non-overlapping tissue expression Patterns. *Front. Plant Sci.* 8, 2175.
- Oldroyd, G.E., Downie, J.A., 2008. Coordinating nodule morphogenesis with rhizobial infection in legumes. *Annu. Rev. Plant Biol.* 59, 519–546.
- Pedretti, M., et al., 2020. SAC3B is a target of CML19, the centrin 2 of *Arabidopsis thaliana*. *Biochem. J.* 477 (1), 173–189.
- Perochon, A., et al., 2011. Calmodulin and calmodulin-like proteins in plant calcium signaling. *Biochimie* 93 (12), 2048–2053.
- Pirayesh, N., et al., 2021. Organellar calcium signaling in plants: an update. *Biochim. Biophys. Acta, Mol. Cell Res.* 1868 (4), 118948.
- Qin, T., et al., 2012. Characterization of the role of calcium in regulating the microtubule-destabilizing activity of MDP25. *Plant Signal. Behav.* 7 (7), 708–710.
- Rayapuram, N., et al., 2014. Identification of novel PAMP-triggered phosphorylation and dephosphorylation events in *Arabidopsis thaliana* by quantitative phosphoproteomic analysis. *J. Proteome Res.* 13 (4), 2137–2151.
- Sattler, M., Schleucher, J., Griesinger, C., 1999. Heteronuclear multidimensional NMR experiments for the structure determination of proteins in solution employing pulsed field gradients. *Prog Nucl Magn Reson* 34 (2), 93–158.
- Schmieder, P., et al., 1994. Improved resolution in triple-resonance spectra by nonlinear sampling in the constant-time domain. *J. Biomol. NMR* 4 (4), 483–490.
- Spyrakakis, F., et al., 2011. Histidine E7 dynamics modulates ligand exchange between distal pocket and solvent in AHb1 from *Arabidopsis thaliana*. *J. Phys. Chem. B* 115 (14), 4138–4146.
- Su, C., et al., 2020. The medicago truncatula DREPP protein triggers microtubule fragmentation in membrane nanodomains during symbiotic infections. *Plant Cell* 32 (5), 1689–1702.
- Takasaki, A., et al., 1999. Identification of the calmodulin-binding domain of neuron-specific protein kinase C substrate protein CAP-22/NAP-22. Direct involvement of protein myristoylation in calmodulin-target protein interaction. *J. Biol. Chem.* 274 (17), 11848–11853.
- Tanaka-Takada, N., et al., 2019. Plasma membrane-associated  $\text{Ca}^{2+}$ -binding protein PCaP1 is involved in root Hydrotropism of *Arabidopsis thaliana*. *Plant Cell Physiol.* 60 (6), 1331–1341.
- Tidow, H., Nissen, P., 2013. Structural diversity of calmodulin binding to its target sites. *FEBS J.* 280 (21), 5551–5565.
- Trande, M., et al., 2019. Cation and peptide binding properties of CML7, a calmodulin-like protein from *Arabidopsis thaliana*. *J. Inorg. Biochem.* 199, 110796.
- Troilo, F., et al., 2022. Rapid kinetics of calcium dissociation from plant calmodulin and calmodulin-like proteins and effect of target peptides. *Biochem. Biophys* 590, 103–108.
- Udenwobebe, D.I., et al., 2017. Myristoylation: an important protein modification in the immune response. *Front. Immunol.* 8.
- Vallet, A., et al., 2023. The plasma membrane-associated cation-binding protein PCaP1 of *Arabidopsis thaliana* is a uranyl-binding protein. *J. Hazard Mater.* 446, 130668.
- Vallone, R., et al., 2016. Metal binding affinity and structural properties of calmodulin-like protein 14 from *Arabidopsis thaliana*. *Protein Sci.* 25 (8), 1461–1471.
- Vandelle, E., et al., 2018. Identification, characterization, and expression analysis of calmodulin and calmodulin-like genes in grapevine (*Vitis vinifera*) reveal likely roles in stress responses. *Plant Physiol. Biochem.* 129, 221–237.
- Vijayapalani, P., et al., 2012. Interaction of the trans-frame potyvirus protein P3N-PIPO with host protein PCaP1 facilitates potyvirus movement. *PLoS Pathog.* 8 (4), e1002639.
- Vosolobě, S., Petrášek, J., Schwarzerová, K., 2017. Evolutionary plasticity of plasma membrane interaction in DREPP family proteins. *Biochim. Biophys. Acta, Biomembr.* 1859 (5), 686–697.
- Vranken, W.F., et al., 2005. The CCPN data model for NMR spectroscopy: development of a software pipeline. *Proteins* 59 (4), 687–696.
- Wang, B., et al., 2021. Protein N-myristoylation: functions and mechanisms in control of innate immunity. *Cell. Mol. Immunol.* 18 (4), 878–888.
- Xu, T., Niu, J., Jiang, Z., 2022. Sensing mechanisms: calcium signaling mediated abiotic stress in plants. *Front. Plant Sci.* 13, 925863.
- Yang, T., Poovaiah, B.W., 2003. Calcium/calmodulin-mediated signal network in plants. *Trends Plant Sci.* 8 (10), 505–512.
- Yang, P., et al., 2022. MDP25 mediates the fine-tuning of microtubule organization in response to salt stress. *J. Integr. Plant Biol.* 64 (6), 1181–1195.
- Yap, K.L., et al., 2000. Calmodulin target Database. *J. Struct. Funct. Genom.* 1 (1), 8–14.
- Yin, C., et al., 2017. *Arabidopsis* RabF1 (ARA6) is involved in salt stress and dark-induced senescence (DIS). *Int. J. Mol. Sci.* 18 (2).
- Ying, J., et al., 2017. Sparse multidimensional iterative lineshape-enhanced (SMILE) reconstruction of both non-uniformly sampled and conventional NMR data. *J. Biomol. NMR* 68 (2), 101–118.